ELSEVIER

Physica B 249–251 (1998) 527–533

PHYSICA B

Terahertz dynamics in confined magnetoexcitons

J. Kono[a,b,*], M.Y. Su[b], J. Černe[1b], M.S. Sherwin[b], S.J. Allen, Jr.[b], T. Inoshita[a], T. Noda[c], H. Sakaki[a]

[a] *Quantum Transition Project, Japan Science and Technology Corporation, Tokyo 153, Japan*
[b] *Center for Terahertz Science and Technology and Department of Physics, University of California, Santa Barbara, CA 93106, USA*
[c] *Institute of Industrial Science, University of Tokyo, Tokyo 106, Japan*

Abstract

We have investigated the linear and nonlinear response of confined magnetoexcitons to intense terahertz (THz) radiation. By monitoring photoluminescence from THz-driven GaAs quantum wells, we have observed for the first time *internal transitions* in direct excitons. The spectrum of excitations is enriched by the complexities of the valence band and is well explained by an effective-mass theory. At high THz-field strengths, the emission properties of the driven quantum wells are completely dominated by new near-band-gap features, or *optical sidebands*, which appear at frequencies $\omega_{NIR} \pm 2n\omega_{THz}$, where ω_{NIR} is the exciton-creation frequency, ω_{THz} is the driving frequency, and n is an integer. The intensity of the sidebands exhibits pronounced enhancement when ω_{THz} coincides with one- and two-photon exciton internal transitions, providing new and accurate information on the internal dynamics of excitons.

Keywords: Free-electron lasers; Terahertz dynamics; Excitons; Optical sidebands

1. Introduction

The states of a quantum system can be "dressed" by interaction with intense oscillating fields. Optical-field-induced line broadening, shifts, and splittings – generally known as the dynamical or AC Stark effect – have been widely studied in atoms driven by intense laser radiation [1].

Excitons have discrete internal energy levels, behaving as "atoms" in semi-conductors. Because of their large spatial extent, these quasi-atoms have very large oscillator strengths compared to real atoms. Transitions between these atom-like levels lie in the far-infrared (FIR)/terahertz (THz) frequency range. Therefore, excitons in an intense THz laser field provide an ideal system in which to study strong light-matter interaction in a regime inaccessible in atomic spectroscopy.

* Corresponding author; Present Address: Stanford University, W.W. Hansen Experimental Physics Laboratory, Stanford FEL Center, MC: 4085, Stanford, CA 94305-4085, USA. Fax: 650 725 8311; e-mail: kono@stanford.edu.

[1] Present Address: Department of Physics, University of Maryland, College Park, MD 20742, USA.

0921-4526/98/$19.00
PII: S0921-4526(98)00179-3

However, very limited research has succeeded in exploring the THz response of excitons [2,3]. This is due to the dilute nature of excitons, which has precluded direct THz absorption studies. In addition, the rarity of sources for intense and coherent radiation in this frequency range has kept it difficult to perform nonlinear THz spectroscopy.

In this paper, we describe results of near-infrared (NIR) – THz two-color spectroscopy of confined magnetoexcitons. The results reveal for the first time both linear and nonlinear THz transitions between magnetically tuned exciton internal levels. At high THz fields, the emission spectrum of the system is completely dominated by THz-field-induced features, or *optical sidebands*.

2. Samples

We studied two MBE-grown QW samples. Sample 1 (2) consisted of 50 (25) periods of undoped $GaAs/Al_{0.3}Ga_{0.7}As$ (10 nm/15 nm) multiple QWs. Sample 2 was grown on 30 periods of $GaAs/Al_{0.69}Ga_{0.31}As$ (4 nm/40 nm) etch-stop layers. We selectively etched off the substrate of sample 2 for NIR transmission spectroscopy.

3. Experimental methods

Intense (< 20 kW) and tunable (0.12–4.75 THz) radiation was provided by the UCSB free-electron lasers (FELs). In linear optically detected THz resonance (ODTR) spectroscopy [2,3], an Ar^+ laser or a tunable cw Ti : Sapphire laser was used to create excitons. The resulting photoluminescence (PL) was detected by a photomultiplier tube (PMT) or an image-intensified CCD camera. The output of the excitation laser was modulated to produce a 50 μs pulse that coincided with the 10 μs THz pulse at the sample. The change in PL induced by THz radiation was recorded as a function of magnetic field, B. For sideband generation, we used a transmission geometry in which NIR radiation from the Ti : Sapphire laser and THz radiation from the FELs passed through the sample collinearly. The transmitted NIR radiation, containing the sidebands, was detected by the CCD.

4. Experimental results

4.1. Linear spectroscopy of internal excitonic transitions

Fig. 1 shows a typical ODTR spectrum obtained for sample 1. Here the amplitude of the heavy-hole (HH) exciton PL in the presence of THz radiation with a frequency of 103 cm^{-1} is plotted against B. The PL amplitude is normalized to that in the absence of THz radiation. Whenever the THz radiation is absorbed resonantly by the system, the PL amplitude decreases resonantly. Three THz resonances are clearly observed. Through detailed comparison with theory [4], we have assigned these resonances to $1s \rightarrow 3p_-[(0\,0) \rightarrow (1\,2)]$, $1s \rightarrow 2p_-(0\,0) \rightarrow (1\,0)]$, and $2p_- \rightarrow 2s[(0\,1) \rightarrow (1\,1)]$ trantions in the low-field hydrogenic [high-field Landau] notation, represented by the dotted, dashed, and solid arrows, respectively, in the figure.

The above data were obtained using a single-channel system, i.e., a PMT with a monochromator. The monochromator was set to detect the peak of the HH PL. At each B, the monochromator was adjusted to follow the diamagnetic shift of the PL peak. Use of a CCD camera has not only drastically increased the data acquisition rate but also revolutionized the type of measurements

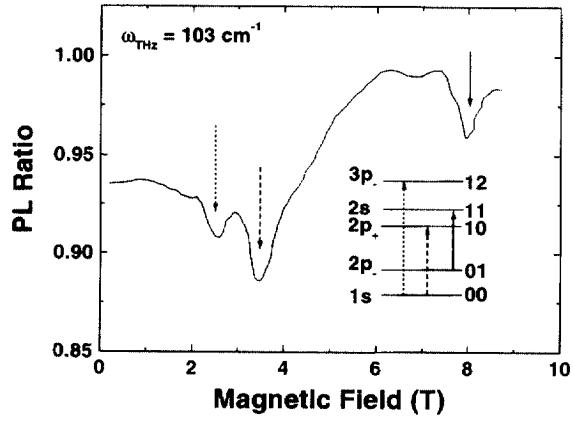

Fig. 1. The ratio of the PL amplitude with and without THz irradiation as a function of magnetic field for sample 1 at a THz frequency of 103 cm^{-1}. Three internal excitonic transitions are clearly observed. The inset shows the origins of these transitions, as discussed in Section 5.1.

that could be made, providing new insight into the mechanisms of ODTR [5,6]. Fig. 2 is a good example of the vast information provided by this *multichannel* ODTR spectroscopy. In this figure the difference of the PL spectra with and without THz irradiation is plotted as a function of B. There are strong qualitative differences in the PL modulation at different B. At 0 T, the difference spectrum shows the expected [7] quenching of the HH PL peak amplitude (labeled A in Fig. 2), the enhancement of the high-energy tail of the HH PL (B), and the enhancement of the light-hole (LH) PL amplitude (C). The HH PL amplitude is resonantly quenched at the $1s \rightarrow 2p_+$ HH resonance at 3.5 T (D and E), while the LH PL reaches a maximum (F). Above 3.5 T very little quenching occurs, and the dominant effect of THz radiation is to enhance and blueshift the HH PL peak (G).

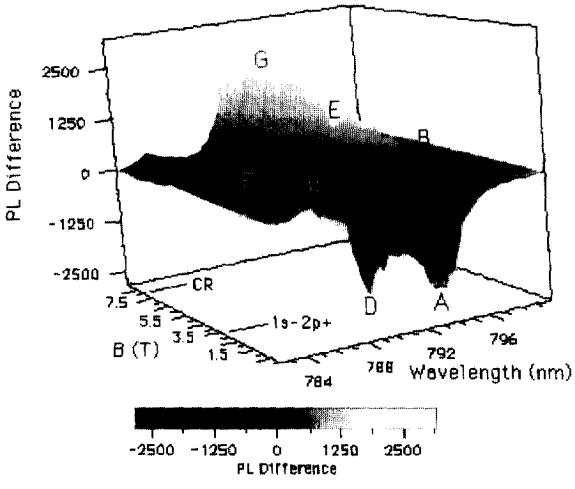

Fig. 2. PL spectra without THz irradiation subtracted from PL spectra with THz irradiation as a function of B.

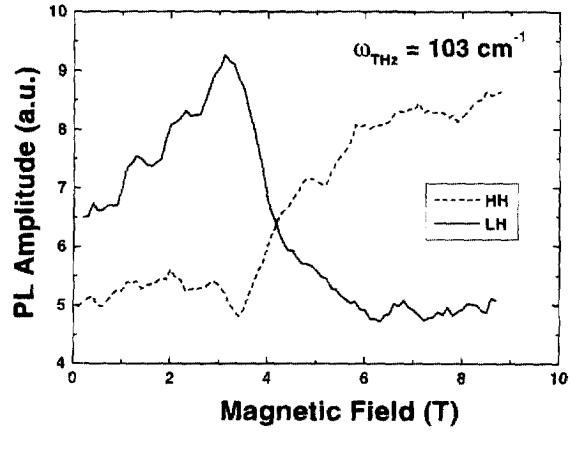

Fig. 3. LH and HH PL amplitudes as a function of B under THz illumination.

The information contained in Fig. 2 is more digestible when cross sections through this surface plot are examined. As an example, the resonant enhancement of the LH PL peak at the expense of the HH PL amplitude is shown in Fig. 3, where the HH and LH PL amplitudes are plotted against B. Note the asymmetry of the LH PL enhancement, with a fast decay above 3.5 T, and a more gradual decrease below 3.5 T. Such information is completely lost in single-channel ODTR, where we monitor only one PL feature.

4.2. *Nonlinear spectroscopy of internal excitonic transitions*

We have investigated the *nonlinear* THz response of magnetoexcitons using a *double-resonance* scheme. The excitons are created resonantly by tunable NIR radiation from a Ti : Sapphire laser, and one- and two-photon exciton internal transitions are resonantly driven by intense THz radiation from the UCSB FELs. The nonlinearity originating from the exciton-THz-photon interaction has resulted in mixing of NIR and THz radiation, which generated strong near-band-gap emission lines, or *optical sidebands*.

Fig. 4a and b show typical sideband spectra at $B = 10$ T obtained for sample 2. The frequency of the THz radiation was 115 cm^{-1} for both figures. In Fig. 4a NIR radiation resonantly creates the 2s [or (1 1) in the high-field notation] HH excitons at 12 745 cm^{-1}. A strikingly narrow emission line, the -2ω sideband, is seen at *exactly* 12 515 cm^{-1} ($=12\,745 - 2 \times 115$ cm^{-1}) only in the presence of THz radiation. The 1s [or (0 0)] HH exciton PL is weaker than the -2ω sideband by about three orders of magnitude, so that it is invisible in this scale. In Fig. 4b, the up-converted sidebands, the $+2\omega$ and $+4\omega$ sidebands, are seen above the NIR fundamental, which resonantly excites the 1s

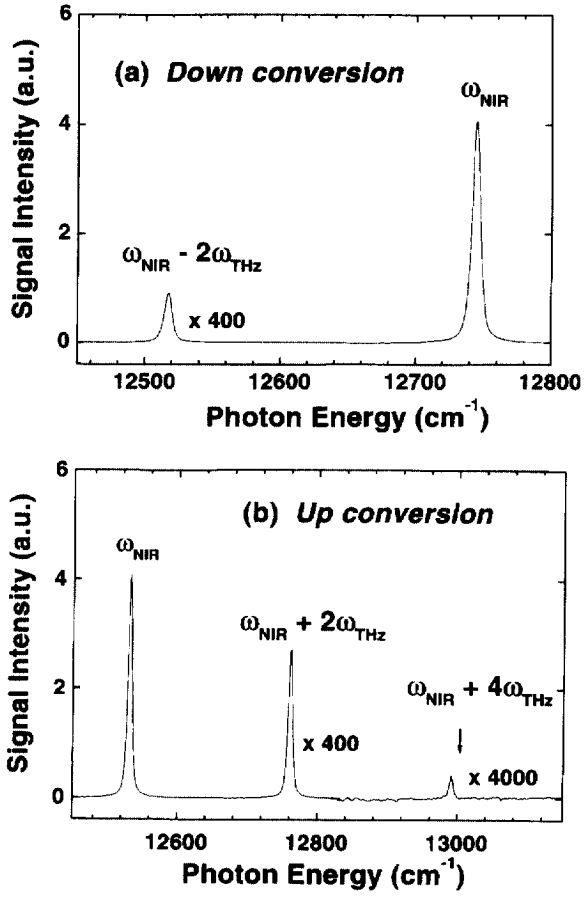

Fig. 4. Typical sideband generation spectra at $B = 10$ T. $\omega_{THz} = 115\ cm^{-1}$ for both figures. (a) Down conversion: $\omega_{NIR} = \omega_{2s} = 12\,745\ cm^{-1}$ and $\omega_{sideband} = \omega_{NIR} - 2\omega_{THz} = 12\,515\ cm^{-1}$. (b) Up conversion: $\omega_{NIR} = \omega_{1s} = 12\,515\ cm^{-1}$, and $\omega_{sideband} = \omega_{NIR} + 2\omega_{THz} = 12\,745\ cm^{-1}$, and $\omega_{NIR} + 4\omega_{THz} = 12975\ cm^{-1}$.

HH excitons at 12 531 cm^{-1}. The typical intensities of the -2ω, $+2\omega$, and $+4\omega$ sidebands are 0.05%, 0.15%, and 0.0015%, respectively, of the incident intensity of the fundamental, which was, in this case, about 100 mW/cm^2. The $+4\omega$ sideband was observed only at the highest THz intensity.

In order to deduce the order of the nonlinear interaction that produced the sidebands, we studied in detail the dependence of the intensity of the $+2\omega$ sideband on the powers of the incident NIR and THz beams [5]. The intensity of the $+2\omega$ sideband increased *quadratically* with increasing THz power for a constant NIR power, whereas for a constant THz power the sideband intensity increased *linearly* with NIR power. Thus we conclude that the $+2\omega$ sideband emission is a third-order nonlinear optical process involving one NIR photon and two THz photons, described by $\boldsymbol{P}(\omega_{NIR} + 2\omega_{THz}) = \chi^{(3)}(\omega_{NIR} + 2\omega_{THz}, \omega_{THz}, \omega_{NIR})E^2_{THz}(\omega_{THz})E_{NIR}(\omega_{THz})$, as discussed in more detail in Section 5.2. Here $\boldsymbol{P}$ is the polarization induced by the laser fields $\boldsymbol{E}_{THz}$ and $\boldsymbol{E}_{NIR}$, and $\chi^{(3)}$ is a third-order nonlinear susceptibility tensor. The same conclusion can be drawn for the -2ω sideband from power-dependence studies, but we have not been able to perform systematic studies on the $+4\omega$ sideband because of its small intensity.

The sideband emission is strongly dependent on the polarization of the THz beam [5]. We continuously changed the degree of circular polarization of the THz beam while monitoring the intensity of the $+2\omega$ sideband at $B = 10$ T for $\omega_{NIR} = 12\,531\ cm^{-1}$ and $\omega_{THz} = 115\ cm^{-1}$. The NIR laser beam was linearly polarized (horizontal direction). The sideband intensity was strongest when the THz radiation was linearly polarized (parallel to the NIR polarization), decreased with increasing degree of circular polarization, and became weakest ($\sim 30\%$ of the strongest) when the THz radiation was circularly polarized. This strongly suggests *that in order to produce the $+2\omega$ sideband there must be both right (σ^+ or electron-CR-active) and left (σ^- or electron-CR-inactive) circularly polarized THz radiation.*

In Fig. 5 the intensity of the $+2\omega$ sideband is plotted as a function of B for $\omega_{THz} = 115\ cm^{-1}$ with $\omega_{NIR} = \omega_{1s}$ at all magnetic fields, where ω_{1s} is the creation frequency for 1s HH excitons. The data demonstrates novel *nonlinear* optically detected THz resonances. There are three distinct resonances at 4.5, 9.5, and 11.5 T, labeled as (a)–(c), respectively. These resonances occur when (a) $\omega_{THz} = \omega_{2p+} - \omega_{1s}$, (b) $2\omega_{THz} = \omega_{2s} - \omega_{1s}$, and (c) $\omega_{THz} = \omega_{2p-} - \omega_{1s}$, in the low-field hydrogenic notation. The resonance positions are in excellent agreement with those expected from the linear ODTR spectroscopy described in Section 4.1 and theory [4] on magnetoexcitons in 10 nm-wide GaAs QWs. Note that the two-photon resonance (b) is forbidden in linear ODTR.

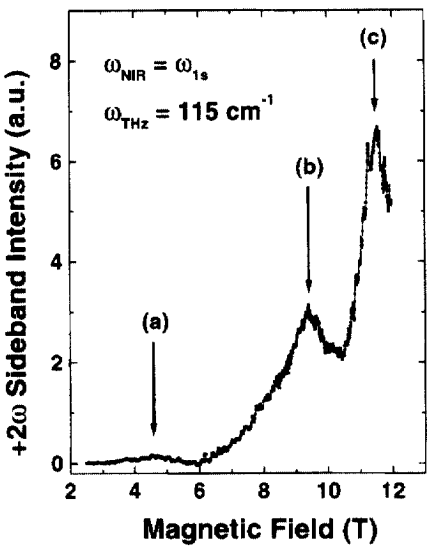

Fig. 5. The magnetic field dependence of the $+2\omega$ sideband intensity for $\omega_{THz} = 115\,cm^{-1}$ and $\omega_{NIR} = \omega_{1s}$ at all magnetic fields. The data demonstrates the first observation of *nonlinear* optically detected THz resonances in confined magnetoexcitons. Pronounced resonances occur when (a) $\omega_{THz} = \omega_{2p+} - \omega_{1s}$, (b) $2\omega_{THz} = \omega_{2s} - \omega_{1s}$, and (c) $\omega_{THz} = \omega_{2p-} - \omega_{1s}$.

We also studied in detail how the intensity of the $\pm 2\omega$ sidebands varies with ω_{NIR} at a constant magnetic field, both experimentally and theoretically [8]. We found that the sideband intensity is resonantly enhanced whenever either ω_{NIR} or $\omega_{NIR} \pm 2\omega_{THz}$ is resonant with an interband exciton-creation frequency such as ω_{1s} and ω_{2s}. The strongest $+2\omega$ sideband was observed when we satisfied the double-resonance condition, $\omega_{NIR} = \omega_{1s}$ and $\omega_{NIR} + 2\omega_{THz} = \omega_{2s}$. Similarly, the strongest -2ω sideband was obtained when $\omega_{NIR} - 2\omega_{THz} = \omega_{1s}$ and $\omega_{NIR} = \omega_{2s}$. These resonance conditions obtained in energy scans, as well as those obtained in magnetic field scans (Fig. 5), are well explained within our perturbation theory, which will be discussed in Section 5.2.

5. Discussion

5.1. Linear spectroscopy of internal exciton transitions

Three quantum numbers specify a state of 2D excitons: the principal quantum number n, the angular momentum projection m_z, and the

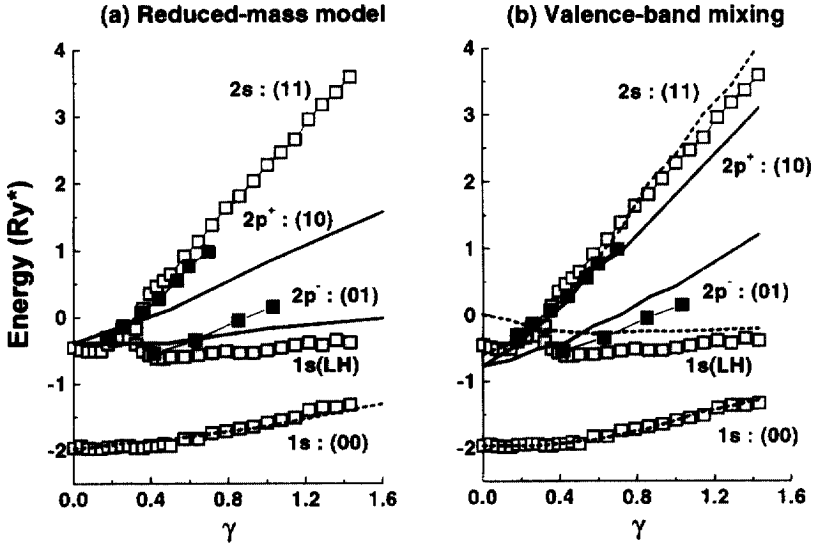

Fig. 6. Low-lying energy levels versus $\gamma = \hbar\omega_c/2R^*$ for excitons in 10 nm-wide GaAs QWs. Solid squares (s-states) – data from interband transitions, open squares (p-states) – data from THz intraband transitions, dashed lines – theory for s-states, and solid lines – theory for p-states. Theory: (a) Ref. [10] and (b) Ref. [3].

center-of-mass momentum $\boldsymbol{K}$. Here we concentrate on the immobile ($\boldsymbol{K} = 0$) excitons since these are the relevant optically-active exciton states [4,9]. In high B, more convenient notation is (N,M), where N (M) represents the electron (hole) Landau index. The low-B–high-B correspondence is given by $n = \max(N,M) + 1$ and $m_z = N - M$, e.g., $1s$: $(n,m_z) = (10) \leftrightarrow (N,M) = (00)$, $2p_+ : (11) \leftrightarrow (10)$, etc. [10]. For σ^+ polarization, e.g., $1s \rightarrow 2p_+$ $[(00) \rightarrow (10)]$, $1s \rightarrow 3p_+$ $[(00) \rightarrow (21)]$, and $2p_- \rightarrow 2s$ $[(01) \rightarrow (11)]$ transitions are expected. It is clear from these that the $1s \rightarrow 2p_+ (1s \rightarrow 2p_-)$ transition is the Coulomb-shifted electron (hole) cyclotron resonance.

In real systems, because of the valence-band mixing, deviation from the above-described simple theory is expected. In Fig. 6 the four low-lying HH exciton levels (1s, $2p_\pm$, 2s) and the lowest LH exciton level (1s), deduced from interband (s-states) and intraband (p-states) transitions, are compared with two different theories. The first theory [11] is a hydrogenic, reduced-mass theory, containing the reduced mass of the e–h pairs as the adjustable parameter. By setting this parameter to an unrealistically large value ($\sim 0.1 m_0$), we can approximately fit the 1s HH state. However, with the same mass, the slopes versus B for the $2p_+$ and $2p_-$ HH states are too small to fit the data, as can be seen in Fig. 6a. The theoretical curves in Fig. 6b were obtained from a paper by Bauer and Ando [4], who calculated energy levels of magnetoexcitons in 10 nm-wide GaAs QWs, taking into account the valence-band complexities within the effective-mass approximation. This theory does not contain any adjustable parameter, so that we simply compared the experiment and theory. The obtained excellent agreement shown in Fig. 6b clearly shows the correctness of the experiment and theory, providing accurate information on these energy levels.

5.2. Nonlinear spectroscopy of internal exciton transitions

The $\pm 2\omega$ sideband generation can be described in terms of a third-order nonlinear susceptibility $\chi^{(3)}_{ijkl}$ defined by $P_i(\omega_{\mathrm{NIR}} \pm 2\omega_{\mathrm{THz}}) = \Sigma_{jkl}\ \chi^{(3)}_{ijkl} E_j(\pm \omega_{\mathrm{THz}}) E_k(\pm \omega_{\mathrm{THz}}) E_l(\omega_{\mathrm{NIR}})$, where $\boldsymbol{P}(\omega)$ and $\boldsymbol{E}(\omega)$ are the Fourier components of the polarization $\boldsymbol{P}(t)$ and the photon electric field $\boldsymbol{E}(t)$, respectively. [$\boldsymbol{P}(t) = \Sigma_\omega \boldsymbol{P}(\omega) e^{-i\omega t}$, etc.] We have developed a perturbation theory which successfully explains the observed phenomena. In the case of the $+2\omega$ sideband, standard perturbation techniques with the exciton–photon interaction $-\boldsymbol{p} \cdot \boldsymbol{E}$ ($\boldsymbol{p}$ is the exciton polarization operator) lead to the following expression for $\chi^{(3)}$:

$$\chi^{(3)}_{ijkl} = \frac{-N_{\mathrm{well}}}{\hbar^3} \sum_{\alpha\beta\gamma} \frac{\langle 0|p_i|\gamma\rangle\langle\gamma|p_j|\beta\rangle\langle\beta|p_k|\alpha\rangle\langle\alpha|p_l|0\rangle}{(\omega_{\mathrm{NIR}} + 2\omega_{\mathrm{THz}} - \omega_\gamma - i\Gamma)(\omega_{\mathrm{NIR}} + \omega_{\mathrm{THz}} - \omega_\beta - i\Gamma)(\omega_{\mathrm{NIR}} - \omega_\alpha + i\Gamma)} + (\text{nonresonant terms}). \tag{1}$$

(The expression for the -2ω sideband is obtained by simply replacing ω_{THz} by $-\omega_{\mathrm{THz}}$.) Here N_{well} is the well-layer density; α, β, and γ run over the exciton states; $\omega_\alpha = (E_\alpha - E_0)/\hbar$ where E_α (E_0) is the energy of the exciton state $|\alpha\rangle$ (vacuum state $|0\rangle$); and Γ is a phenomenological damping factor.

Eq. (1) indicates that $\chi^{(3)}$ is resonantly enhanced when (A) $\omega_{\mathrm{NIR}} = \omega_{\mathrm{ns}}$, (B) $\omega_{\mathrm{NIR}} + \omega_{\mathrm{THz}} = \omega_{\mathrm{n'pm}}$ ($m = \pm 1$), or (C) $\omega_{\mathrm{NIR}} + 2\omega_{\mathrm{THz}} = \omega_{\mathrm{n''s}}$. These resonance conditions agree with the experimental observations and can be well visualized by using the diagrams shown in Fig. 7a–c. In the figures the dashed lines are intermediate *virtual* levels that exist only when the material system is interacting with the laser fields, whereas the solid lines are *real* magneto-excitonic levels such as $|1s\rangle$, $|2s\rangle$, and $|2p_\pm\rangle$. If one of the real levels is nearly coincident with one of the virtual levels, resonant enhancement of $\chi^{(3)}$ occurs. In all the three cases, (a)–(c), two of the above three conditions (A)–(C) are satisfied: (a) $\omega_{\mathrm{NIR}} = \omega_{1s}$, $\omega_{\mathrm{NIR}} + \omega_{\mathrm{THz}} = \omega_{2p-}$, (b) $\omega_{\mathrm{NIR}} = \omega_{1s}$, $\omega_{\mathrm{NIR}} + 2\omega_{\mathrm{THz}} = \omega_{2s}$, and (c) $\omega_{\mathrm{NIR}} = \omega_{1s}$, $\omega_{\mathrm{NIR}} + \omega_{\mathrm{THz}} = \omega_{2p-}$. In (b) [(c)] the detuning of the

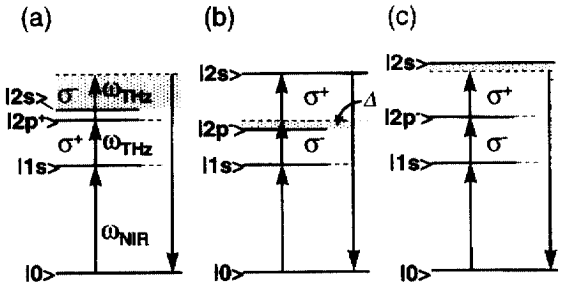

Fig. 7. Diagrammatic representation of the resonant processes responsible for the observed three resonances in Fig. 5. The dashed lines represent virtual levels, whereas the solid lines represent real magneto-excitonic levels. Resonances occur when real levels coincide with virtual levels. The shaded area represents the magnitude of the detuning Δ.

remaining unsatisfied condition $\Delta = (\omega_{NIR} + \omega_{THz}) - \omega_{2p-}[\Delta = (\omega_{NIR} + 2\omega_{THz}) - \omega_{2s}]$ is also small (less than 10 cm^{-1}), consistent with the observed large peaks (see Fig. 5). On the other hand, the large detuning ($> 100\ cm^{-1}$) in (a) results in the small peak intensity as seen in Fig. 5.

Eq. (1) also explains the observed THz polarization dependence of the sideband intensity. Let us consider the case where $|\alpha\rangle = |1s\rangle$, $|\beta\rangle = |2p_-\rangle$, and $|\gamma\rangle = |2s\rangle$. If the THz radiation is left circularly polarized (σ^-), it can induce the $1s \rightarrow 2p_-$ transition, but then it cannot induce the subsequent $2p_- \rightarrow 2s$ transition due to angular momentum conservation, leading to vanishing sideband intensity. Similarly, for a THz photon of the opposite helicity (σ^+), the first transition is forbidden while the second is allowed. On the other hand, the sideband intensity is maximum for linearly polarized THz radiation, which is an equal-weight mixture of circular polarizations of opposite helicities, consistent with the experimental results.

In summary, we report results of a new type of NIR–THz two-color optical experiments on the internal structure and dynamics of confined excitons using a cw Ti : Sapphire laser and the UCSB free-electron lasers as the sources. Both linear and nonlinear exciton internal transitions were directly probed for the first time. The power of multichannel detectors in ODTR spectroscopy was clearly revealed. Strong near-band-gap emission lines, or optical sidebands, were observed for the first time in undoped GaAs/AlGaAs QWs at high magnetic fields. We have developed a perturbation theory which successfully explains the observed behavior of the sidebands. Currently, we are working toward further higher THz-field regimes, where the above presented perturbation scheme should break down and a nonperturbative "dressed" exciton picture is required.

Acknowledgements

This work was supported by JST Quantum Transition Project, ONR N00014-K-0692, and QUEST DMR91-20007. The authors are grateful to T. Ando, G.E.W. Bauer, A.B. Dzyubenko, A. Imamoglu, K. Johnsen for useful comments and discussions, and D.P. Enyeart, D.T. White and J.R. Allen at CTST for technical support.

References

[1] See, e.g., S. Feneuille, Rep. Prog. Phys. 40 (1977) 1257.
[2] J. Černe, J. Kono, M.S. Sherwin, M. Sundaram, A.C. Gossard, G.E.W. Bauer, Phys. Rev. Lett. 77 (1996) 1131 and references therein.
[3] See also M.S. Salib et al., Phys. Rev. Lett. 77 (1996) 1135.
[4] G.E.W. Bauer, T. Ando, Phys. Rev. B 38 (1988) 6015.
[5] For a more detailed account, see J. Kono et al., in Proc. SPIE Vol. 3153 (1997) 96.
[6] Similar work using a CCD camera has been recently reported: G.S. Herold et al., Proc. 8th Int. Conf. on Modulated Semiconductor Structures, Santa Barbara, USA. July 1997, to be published in Physica E 2 (1998).
[7] J. Černe et al., Phys. Rev. B 51 (1995) 5253.
[8] T. Inoshita, J. Kono, H. Sakaki, Phys. Rev. B 57 (1998) 4604.
[9] A.B. Dzyubenko, A.L. Yablonskii, Pis'ma Zh. Eksp. Teor. Fiz. 64 (1996) 198 [JETP Lett. 64 (1996) 213].
[10] A.H. MacDonald, D.S. Ritchie, Phys. Rev. B 33 (1986) 8336.
[11] R.L. Greene, K.K. Bajaj, Phys. Rev. B 31 (1985) 913.